



Dynamics of turbid buoyant plumes and the feedbacks on near-shore biogeochemistry and physics

Bronwyn Cahill,^{1,2} Oscar Schofield,² Robert Chant,² John Wilkin,² Eli Hunter,² Scott Glenn,² and Paul Bissett¹

Received 11 February 2008; revised 2 April 2008; accepted 17 April 2008; published 22 May 2008.

[1] The near-shore waters of the New York/New Jersey Bight in April 2005 exhibited distinct regions of turbid water with clearly differing optical properties associated with the Hudson River plume. We examined the effect of variable light attenuation on the hydrodynamics and ecological response of the Hudson River plume and its environs using field observations and a 3-dimensional biophysical model. Important feedback mechanisms between the attenuation of light and the resulting impact on the mixed layer depth were revealed from the modeling results. High concentrations of chlorophyll, detritus and colored dissolved organic matter in the upper water column as a result of enhanced stratification increase the attenuation of light and modify the buoyancy driven circulation. This further impacts the growth of phytoplankton in the model and subsequently modifies the vertical profile of the attenuation coefficient, which in turn feeds back into the overall heat budget. **Citation:** Cahill, B., O. Schofield, R. Chant, J. Wilkin, E. Hunter, S. Glenn, and P. Bissett (2008), Dynamics of turbid buoyant plumes and the feedbacks on near-shore biogeochemistry and physics, *Geophys. Res. Lett.*, 35, L10605, doi:10.1029/2008GL033595.

1. Introduction

[2] The Hudson River represents a major source of total suspended matter, nutrients and chemical contaminants in the Hudson River Bay and beyond into the Mid-Atlantic Bight (Figure 1a). It is a main factor controlling biogeochemical and physical processes in the region. The transport and transformation of these materials are regulated by the dynamics and structure of the Hudson River plume [Chant *et al.*, 2007]. High freshwater discharge events in spring are associated with the seasonal onset of heating and stratification on inner shelf waters, raising the question as to the significance of the feedbacks between the optical characteristics of the water column, the subsequent vertical distribution of heating, baroclinic circulation and biological productivity in these coastal regions.

[3] Understanding the biogeochemical dynamics within a turbid coastal plume is complicated by the feedbacks between the absorption of light by dissolved and particulate material and the corresponding ocean radiant heating in the upper water column. This has been elegantly demonstrated for the open ocean where the upper ocean chlorophyll

concentration regulates the radiant transmission and heating rates in mixed layer depth [Lewis *et al.*, 1990; Morel and Antoine, 1994; Ohlmann *et al.*, 1996, 1998, 2000; Bissett *et al.*, 2001]. Enhanced near-surface stratification positively feedbacks on the phytoplankton growth, which in turn increases near surface local heating [Dickey and Falkowski, 2002]. Ohlmann *et al.* [2000] demonstrated that an increase in chlorophyll concentration from 0.03 mg m⁻³ to 3 mg m⁻³ in the upper 10 m of the water column can decrease the solar flux in surface waters by as much as 35 W m⁻². A 10 W m⁻² change in the solar radiation absorbed within a 10 m layer can represent a temperature change of more than 0.6°C month⁻¹ [Simpson and Dickey, 1981]. Despite these findings, bio-optical modules integrated into ocean models rarely resolve the optical complexity of the coastal ocean where significant amounts of dissolved colored organic carbon and detritus are present [Bissett *et al.*, 2005, 2008]. As part of the Lagrangian Transport and Transformation Experiment (LaTTE), we studied the impact of different water types (river plume versus open shelf) on surface radiant heating and stratification rates to assess the feedbacks between optical turbidity and near-shore physics.

2. Method

2.1. Model Water-Type Classification and Solar Transmission Parameterization

[4] The Paulson and Simpson [1977] formulation of ocean radiant heating is commonly used to parameterize solar transmission in ocean models. The fraction of solar shortwave radiation flux penetrating the water column to a specified depth z is computed as a function of exponential decay,

$$\frac{I_{(z,\lambda)}}{I_{(0,\lambda)}} = R \exp\left(-\frac{z}{\zeta_1}\right) + (1 - R) \exp\left(-\frac{z}{\zeta_2}\right), \quad (1)$$

where the first exponential term of (1) describes the stronger attenuation of light in the red (longwave) part of the spectrum, and the second exponential term describes the weaker attenuation of blue-green (shortwave) part of the spectrum. The coefficients ζ_1 and ζ_2 are attenuation lengths representing longwave and shortwave bands, respectively, and are prescribed in this work as a function of Jerlov water type [Jerlov, 1968]. R describes the relative amount of red light incident on the sea surface. In this work, the different water types were identified by both the total turbidity in the water column and the relative contributions from phytoplankton, detritus and CDOM to the total light absorption values. Absorption contributions by the phytoplankton, detritus, and CDOM were derived by inverting

¹Florida Environmental Research Institute, Tampa, Florida, USA.

²Institute of Marine and Coastal Studies, Rutgers University, New Brunswick, New Jersey, USA.

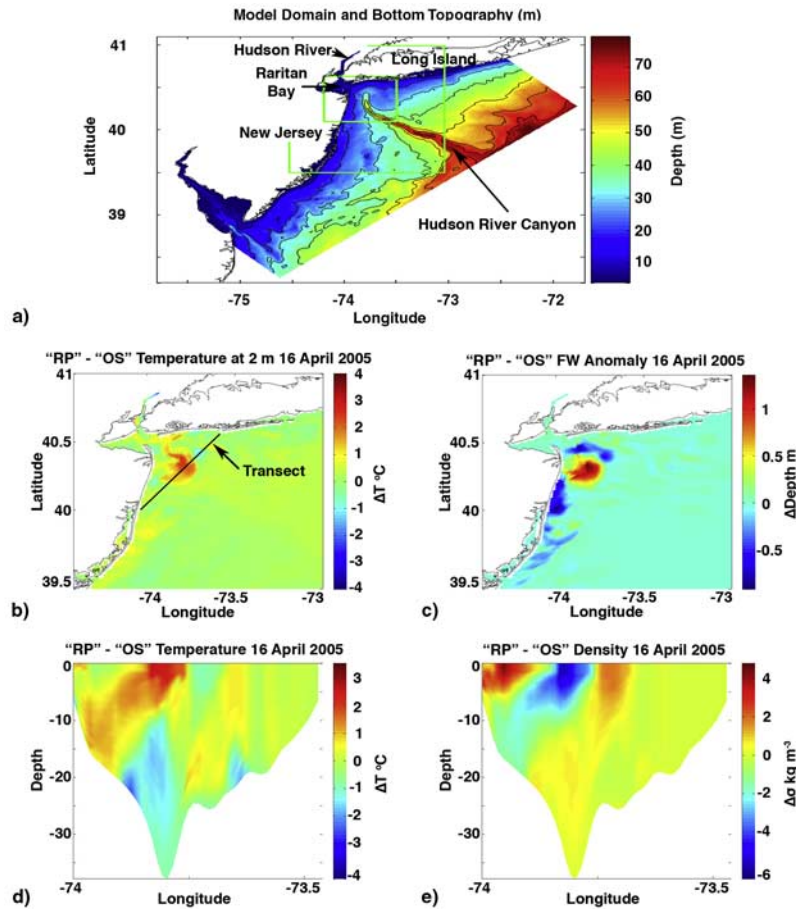


Figure 1. (a) Model domain and bottom topography (green boxes highlight inner and outer areas of interest within model domain), (b, d) “river plume (RP)” – “open shelf (OS)” temperature difference, (c) freshwater anomaly difference, and (e) density anomaly difference 16th April 2005.

absorption data taken in situ with a Wetlabs AC-9 absorption-attenuation meter using a simple optical signature inversion model [Schofield *et al.*, 2004, 2006]. The data show two distinct water types in the study region, with open shelf water situated east of the Hudson River Canyon and river plume water situated south of the mouth of the Hudson River estuary and along the New Jersey coast. Some near-shore mixtures of the two water types are also present. Open shelf water (characterized by small (spectrally integrated) total absorption values, $<0.1 \text{ m}^{-1}$) closely resembles Jerlov water type 3 (coastal waters) and has a 1% light level near 20 m depth, while near shore mixtures and river plume water types (characterized by high total absorption values, $>0.2 \text{ m}^{-1}$) have 1% light levels in the vicinity of 11 m and 5 m depth, respectively.

[5] We compared two simulations that both use the Paulson and Simpson [1977] formulation as the basis for modeling solar transmission. The “open shelf” water type is characterized by a constant attenuation length scale characteristic of coastal water with a 1% light level in the vicinity of 20 m (Table 1). The “river plume” water type is initialized with a base attenuation length scale characteristic of coastal water with a 1% light level around 10 m but light attenuation is scaled dynamically in time and space to

modeled attenuation lengths within the Hudson River plume.

2.2. Regional Ocean Modeling System, ROMS

[6] We use the Regional Ocean Modeling System, ROMS [Haidvogel and Beckmann, 1999; Wilkin *et al.*, 2005] in order to examine the inter-relationship between vertical absorption scales for shortwave radiation, subsequent heating and circulation. The ROMS computational kernel have been described in detail by Shchepetkin and McWilliams [1998, 2003, 2005]. ROMS uses a vertically stretched terrain-following “s-coordinate” with selective weighting of the vertical distribution of points toward the free surface or seafloor, or both. The weighted stretching of the vertical coordinate allows for enhanced resolution in the upper ocean mixed layer and turbulent bottom boundary

Table 1. Base Parameter Values Used to Characterize Different Water Types With Attenuation Length Scales Derived From Inverted Wetlabs AC-9 Absorption Data

	R	ζ_1 , m	ζ_2 , m
Open shelf (constant)	0.58	0.35	23
River plume (variable)	0.50	0.01	4.9

Table 2. River Biology Input Concentrations^a

Biological River Inputs	Concentration, mmol m ⁻³
NO ₃	20
NH ₄	0.1
SiO	4
PO ₄	1.4
DIC	2000
CDM (labile)	1
CDM (relict)	500
DOM (labile)	35
DOM (relict)	550
All other biological variables	0.1

^aJ. Reinfelder (personal communication, 2007).

layer. The horizontal discretization is by an orthogonal curvilinear Arakawa C-grid.

2.3. Ecological Modeling System, EcoSim

[7] EcoSim is an ecological/optical modeling system that was developed for simulations of carbon cycling and biological productivity [Bissett *et al.*, 1999a, 1999b, 2005, 2008]. It includes four phytoplankton functional groups (large diatoms, small diatoms, large dinoflagellates, synechococcus), each with a characteristic pigment suite which vary with the group carbon-to-chlorophyll-*a* ratio, C:Chl_{*a*}. EcoSim spectrally-resolves irradiance fields as opposed to using integrated irradiance. This allows differential growth of different phytoplankton groups that have unique pigment complements. These properties of each functional group evolve over time as a function of light and nutrient conditions. Other EcoSim components include bacteria, dissolved organic matter, dissolved inorganic carbon cycling and 5 nutrients (NO₃, NH₄, PO₄, SiO, FeO). The interaction between EcoSim's components describe autotrophic growth of and competition between the four phytoplankton groups, differential carbon and nitrogen cycling, nitrogen fixation and grazing. The maximum phytoplankton growth is modulated by temperature [Eppley, 1972]. Loss is effected by grazing and excretion. Grazing accounts for the majority of the biomass sink in this model and is considered the closure term of the phytoplankton equations [Steele and Henderson, 1992]. It is modeled as a Michaelis-Menten function based on the functional groups' biomass [Bissett *et al.*, 1999a].

2.4. Model Domain, Boundary Conditions, Initialization and Forcing

[8] We used the LaTTE geographical domain of Choi and Wilkin [2007] which incorporates the lower Hudson River and Hudson River Canyon, extending from central Long Island to the southern tip of New Jersey (Figure 1a). We applied the following changes to the forcing and initial conditions. NCEP NAM 3-hourly re-analysis forecast of u_{10} winds, air temperature, relative humidity, air pressure and downward longwave and shortwave radiation were used to calculate air-sea heat and momentum fluxes using bulk formulae [Fairall *et al.*, 1996, 2003]. River outflow was prescribed using daily mean Hudson River outflow from the United States Geological Survey (USGS) gauges. The model was initialized with historical observations of temperature and salinity. Initial conditions for nitrate were derived using polynomial approximations that predict ni-

trate concentrations as a function of temperature and salinity [Fennel *et al.*, 2006]. All other biological variables were derived using polynomial approximations that predict concentrations as a function of nitrate and/or carbon to chl-*a* ratios. Representative riverine inputs of temperature, salinity, nutrients and dissolved organic and inorganic matter were prescribed by multiplying the freshwater flow by values given in Table 2 (J. Reinfelder, personal communication, 2007).

3. Results

3.1. Modeled Scenarios

[9] We compare two modeled scenarios, the first is referred to as “open shelf” and uses a fixed light attenuation scheme, the second is referred to as “river plume” and uses a variable light attenuation scheme. Our modeled scenarios focus on a high spring freshwater discharge event ($\sim 4300 \text{ m}^3 \text{ s}^{-1}$) and variable wind stress at the beginning of April 2005. Biological response times are typically on the order of a few days to a week and therefore we examined model results between 10 and 20 days following the high discharge event along a cross-section extending from the New Jersey coast at 40.1°N northeast across the tip of the Hudson River Canyon toward Long Island (Figure 1b).

[10] The model runs demonstrate how different parameterizations of downward irradiance $I(z)$ lead to different upper ocean water mass structures (temperature, salinity, density, phytoplankton). The “river plume” scenario (characterized by shorter, variable attenuation lengths) initially results in warmer surface temperatures ($\Delta T \sim +2^\circ\text{C}$) and a deeper and warmer surface mixed layer 13 days after the peak in discharge event. The gradient in temperature with depth is much sharper in the “river plume” simulation, with colder, bottom water persisting at depth ($\Delta T \sim -2^\circ\text{C}$) (Figure 1d), compared to the “open shelf” simulation. Simpson and Dickey [1981] show that at low wind speeds, shorter attenuation lengths in the upper few meters of the water column result in warmer sea surface temperatures, a sharper thermocline and greater velocity shear. This result is evident in the density cross-sections 13 days after the peak in discharge event. A distinctive gradient in the density anomaly structure is observed in the “river plume” simulation compared with the “open shelf” simulations. In the “river plume” model, the front separates a narrow southward buoyancy driven coastal current along the New Jersey coast and an anti-cyclonic circulation around a freshwater bulge at the head of the Hudson River Canyon. Variability in density structure reflects the differences in the evolving temperature and salinity properties between the simulations. Thus, the formation and transport of freshwater in the plume is influenced by variability in light attenuation.

[11] Our bio-optical simulations reflect the high freshwater discharge event ($\sim 4300 \text{ m}^3 \text{ s}^{-1}$) which peaked on the 3rd April 2005 during variable north winds. Consistent with the findings of Choi and Wilkin [2007], transport of freshwater is split into several pathways. In the first few days following the peak in freshwater discharge, there is very little difference in the transport pathways of freshwater between the “open shelf” and “river plume” simulations. In response to a north-northeastward wind stress, four days after the peak in the freshwater discharge event, a re-circulating freshwater

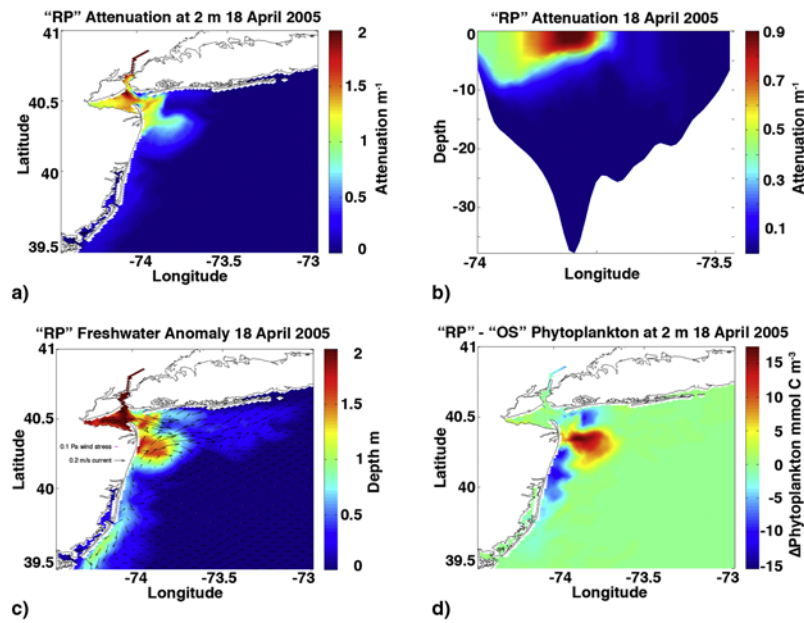


Figure 2. (a, b) “River plume (RP)” attenuation (m^{-1}), (c) freshwater anomaly, and (d) “river plume (RP)” - “open shelf (OS)” phytoplankton difference 18th April 2005.

bulge forms at the mouth of the estuary with flow directed eastward offshore of the New Jersey coast and along the coast of Long Island (not shown). A slackening of the winds and shift in wind direction to the northwest two days later, disperses the re-circulating bulge and pushes freshwater back toward the mouth of the estuary and along the New Jersey coast (not shown). Approximately 10 days after the peak in discharge event, the temperature and phytoplankton biomass of the freshwater anomaly and its transport pathway diverge between the “open shelf” and “river plume” simulations. The divergence in water temperature

between the “river plume” and “open shelf” simulations is initially $\sim 1^\circ\text{C}$ but grows to 2°C , 13 days after the peak in discharge event (Figures 1b and 1d). The increase in temperature anomaly coincides with a shift in wind direction toward the east and a subsequent increase in volume of the freshwater anomaly retained within the bulge at the head of the Hudson River Canyon in the “river plume” simulations (Figure 1c).

[12] The relationship between water temperature, transport of river plume properties and biogeochemical transformations was evident in the different model simulations (Figure 2). The phytoplankton biomass anomaly between

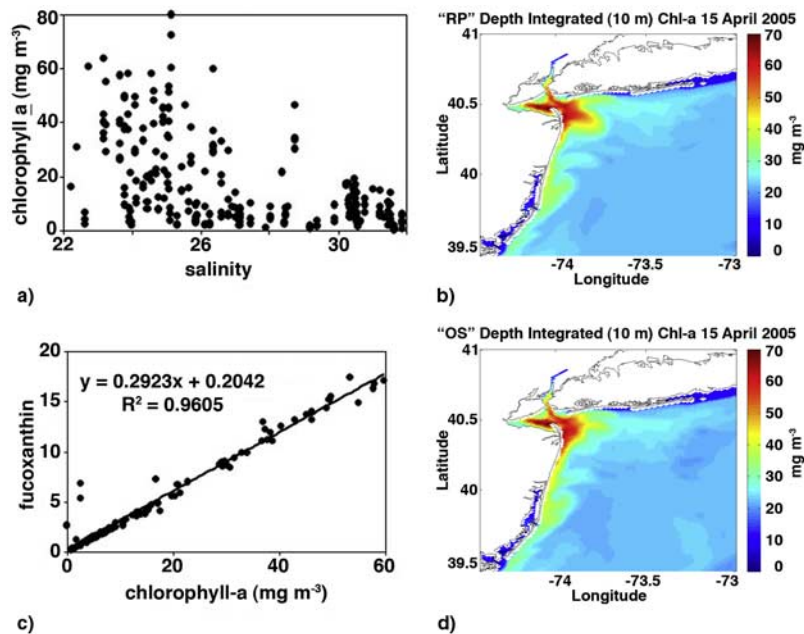


Figure 3. LaTTE April 2005 chl-a (mg m^{-3}) vs. (a) salinity and (c) fucoxanthin, and (b) EcoSim “river plume” and (d) “open shelf” depth integrated (10 m) large diatom chl-a pigments (mg m^{-3}) 15th April 2005.

the model simulations tracks the freshwater anomaly. Phytoplankton growth responds 4 days after the peak in freshwater discharge in both simulations, with the peak in phytoplankton production occurring 11 days later. The bloom remains active for 4 days and then disperses and/or dies. Biomass is gone from the system 20 days after the peak in freshwater discharge event.

3.2. LaTTe 2005 Observations Versus Model Results

[13] Model depth integrated (top 10 m) chlorophyll-a is dominated by diatoms in both “open shelf” and “river plume” simulations. Within plume waters, chlorophyll concentrations peak around 60 mg m^{-3} , while on the shelf they are much smaller, typically $\sim 20 \text{ mg m}^{-3}$ (Figures 3c and 3d). This is consistent with April 2005 observations where chlorophyll-a concentrations exceeded 60 mg m^{-3} within the relatively low salinity waters of the plume and were generally less than 5 mg m^{-3} on the shelf (Figure 3a). Microscopic analyses of Raritan Bay water indicated that the phytoplankton community was dominated by $>100 \mu\text{m}$ chain forming diatoms, primarily *Skeletonema costatum* and *Chaetoceros socialis* sp. (O. Schofield, The Hudson River plume and its role in low dissolved oxygen on the Mid-Atlantic Bight, manuscript in preparation, 2008). Ship chlorophyll-a measurements from April 2005 were highly correlated with fucoxanthin ($R^2 = 0.96$) indicating diatoms dominated these waters during this period (Figure 3b).

4. Discussion

[14] We examined the effect of variable light attenuation scales on the dynamics of the Hudson River plume during a high spring freshwater discharge event using a three-dimensional bio-physical model for the New York/New Jersey Bight. The introduction of variable attenuation of light profiles associated with buoyant plumes in the model altered the surface heat budget by increasing the water temperature and this resulted in changes in the buoyancy driven circulation. This impacted the growth of phytoplankton in the model and subsequently modified the evolution of the attenuation fields, which in turn fed back into the overall heat budget. The method used to introduce variable attenuation into the model in these simulations is simplistic, however it enabled indirect biological feedbacks. These feedbacks altered near-shore physical structure and circulation highlighting that resolving temporal and spatial variability in light attenuation in bio-physical models is critical to modeling biogeochemical and physical processes impacted by turbid coastal plumes.

[15] **Acknowledgments.** This work was supported by the National Science Foundation’s LaTTe (OCE-0238957; OCE-0238745) and ONR MURI (N000140610739) programs. We thank two anonymous reviewers for their helpful comments and suggestions.

References

- Bissett, W. P., J. J. Walsh, D. A. Dieterle, and K. L. Carder (1999a), Carbon cycling in the upper waters of the Sargasso Sea: I. Numerical simulation of differential carbon and nitrogen fluxes, *Deep Sea Res., Part I*, *46*, 205–269.
- Bissett, W. P., K. L. Carder, J. J. Walsh, and D. A. Dieterle (1999b), Carbon cycling in the upper waters of the Sargasso Sea: II. Numerical simulation of apparent and inherent optical properties, *Deep Sea Res., Part I*, *46*, 271–317.
- Bissett, W. P., O. Schofield, S. Glenn, J. J. Cullen, W. L. Miller, A. J. Plueddemann, and C. D. Mobley (2001), Resolving the impacts and feedbacks of ocean optics on upper ocean ecology, *Oceanography*, *14*, 30–53.
- Bissett, W. P., R. Arnone, S. DeBra, D. Dieterle, D. Dye, G. Kirkpatrick, O. Schofield, and G. Vargo (2005), Predicting the optical properties of the West Florida Shelf: Resolving the potential impacts of a terrestrial boundary condition on the distribution of colored dissolved and particulate matter, *Mar. Chem.*, *95*, 199–233.
- Bissett, W. P., R. Arnone, S. DeBra, D. Dye, G. Kirkpatrick, C. Mobley, and O. M. Schofield (2008), The integration of ocean color remote sensing with coastal nowcast/forecast simulations of harmful algal blooms (HABs), in *Real Time Coastal Observing Systems for Ecosystem Dynamics and Harmful Algal Blooms*, edited by M. Babin, C. Roesler, J. J. Cullen, pp. 85–108, U.N. Educ., Sci. and Cult. Organ., Paris.
- Chant, R. J., W. R. Geyer, R. Houghton, E. Hunter, and J. Lerczak (2007), Estuarine boundary layer mixing processes: Insights from dye experiments, *J. Phys. Oceanogr.*, *37*, 1859–1877.
- Choi, B., and J. L. Wilkin (2007), The effect of wind on the dispersal of the Hudson River plume, *J. Phys. Oceanogr.*, *37*, 1878–1897.
- Dickey, T. D., and P. G. Falkowski (2002), Solar energy and its biological-physical interactions in the sea, in *The Sea*, vol. 12, edited by A. R. Robinson, J. J. McCarthy, and B. J. Rothschild, chap. 10, pp. 401–440, John Wiley, Hoboken, N. J.
- Eppley, R. W. (1972), Temperature and phytoplankton growth in the sea, *Fish. Bull.*, *70*(4), 1063–1085.
- Fairall, C. W., E. F. Bradley, D. P. Rogers, J. B. Edson, and G. S. Young (1996), Bulk parameterization of air-sea fluxes for Tropical Ocean-Global Atmosphere Coupled-Ocean Atmosphere Response Experiment, *J. Geophys. Res.*, *101*, 3747–3764.
- Fairall, C. W., E. F. Bradley, J. E. Hare, A. A. Grachev, and J. Edson (2003), Bulk parameterization of air-sea fluxes: Updates and verification for the COARE algorithm, *J. Clim.*, *16*, 571–591.
- Fennel, K., J. Wilkin, J. Levin, J. Moisan, J. O’Reilly, and D. Haidvogel (2006), Nitrogen cycling in the Middle Atlantic Bight: Results from a three-dimensional model and implications for the North Atlantic nitrogen budget, *Global Biogeochem. Cycles*, *20*, GB3007, doi:10.1029/2005GB002456.
- Haidvogel, D. B., and A. Beckmann (1999), *Numerical Ocean Circulation Modeling*, *Ser. Environ. Sci. Manage.*, vol. 2, 318 pp., Imp. Coll. Press, London.
- Jerlov, N. G. (1968), *Optical Oceanography*, 194 pp., Elsevier, Amsterdam.
- Lewis, M. R., M.-E. Carr, G. C. Feldman, W. Esaias, and C. McClain (1990), Influence of penetrating solar radiation on the heat budget of the equatorial Pacific Ocean, *Nature*, *347*, 543–545.
- Morel, A., and D. Antoine (1994), Heating rate within the upper ocean in relation to its bio-optical state, *J. Phys. Oceanogr.*, *24*, 1652–1665.
- Ohlmann, J. C., D. A. Siegel, and C. Gautier (1996), Ocean mixed layer radiant heating and solar penetration: A global analysis, *J. Clim.*, *9*, 2265–2280.
- Ohlmann, J. C., D. A. Siegel, and L. Washburn (1998), Radiant heating of the western equatorial Pacific during TOGA-COARE, *J. Geophys. Res.*, *103*, 5379–5395.
- Ohlmann, J. C., D. A. Siegel, and C. D. Mobley (2000), Ocean radiant heating. part I: Optical influences, *J. Phys. Oceanogr.*, *30*, 1833–1848.
- Paulson, C. A., and J. J. Simpson (1977), Irradiance measurements in the upper ocean, *J. Phys. Oceanogr.*, *7*, 952–956.
- Schofield, O., T. Bergmann, M. J. Oliver, A. Irwin, G. Kirkpatrick, W. P. Bissett, M. A. Moline, and C. Orrico (2004), Inversion of spectral absorption in the optically complex coastal waters of the Mid-Atlantic Bight, *J. Geophys. Res.*, *109*, C12S04, doi:10.1029/2003JC002071.
- Schofield, O., J. Kerfoot, K. Mahoney, M. Moline, M. Oliver, S. Lohrenz, and G. Kirkpatrick (2006), Vertical migration of the toxic dinoflagellate *Karenia brevis* and the impact on ocean optical properties, *J. Geophys. Res.*, *111*, C06009, doi:10.1029/2005JC003115.
- Shchepetkin, A. F., and J. C. McWilliams (1998), Quasi-monotone advection schemes based on explicit locally adaptive dissipation, *Mon. Weather Rev.*, *126*, 1541–1580.
- Shchepetkin, A. F., and J. C. McWilliams (2003), A method for computing horizontal pressure-gradient force in an oceanic model with a nonaligned vertical coordinate, *J. Geophys. Res.*, *108*(C3), 3090, doi:10.1029/2001JC001047.
- Shchepetkin, A. F., and J. C. McWilliams (2005), The regional ocean modeling system: A split-explicit, free-surface, topography following coordinates ocean model, *Ocean Modell.*, *9*, 347–404.
- Simpson, J. J., and T. D. Dickey (1981), The relationship between downward irradiance and upper ocean structure, *J. Phys. Oceanogr.*, *11*, 309–323.
- Steele, J. H., and E. W. Henderson (1992), The role of predation in plankton models, *J. Plankton Res.*, *14*(1), 157–172.
- Wilkin, J. L., H. G. Arango, D. B. Haidvogel, C. S. Lichtenwalner, S. M. Glenn, and K. S. Hedström (2005), A regional ocean modeling system for

the Long-term Ecosystem Observatory, *J. Geophys. Res.*, *110*, C06S91, doi:10.1029/2003JC002218.

R. Chant, S. Glenn, E. Hunter, O. Schofield, and J. Wilkin, Institute of Marine and Coastal Studies, Rutgers University, 71 Dudley Road, New Brunswick, NJ 08901, USA.

P. Bissett and B. Cahill, Florida Environmental Research Institute, 10500 University Center Drive, Suite 140, Tampa, FL 33612, USA. (bronwyn@marine.rutgers.edu)